7th January 2020

Indirect Photo-Electrochemical Detection of Carbohydrates with Pt@g-C_3N_4 Immobilised into a Polymer of Intrinsic Microporosity (PIM-1) and Attached to a Palladium Hydrogen Capture Membrane

Yuanzhu Zhao [1], Joshua Dobson [1], Catajina Harabajiu [1], Elena Madrid [1], Tinakorn Kanyanee [1,2,3], Catherine Lyall [1,4], Shaun Reeksting [1,4], Mariolino Carta [5], Neil B. McKeown [6], Laura Torrente-Murciano [7], Kate Black [8], and Frank Marken [1]*

[1] *Department of Chemistry, University of Bath, Claverton Down, Bath BA2 7AY, UK*
[2] *Department of Chemistry, Faculty of Science, Chiang Mai University, Chiang Mai, 50200, Thailand*
[3] *Center of Excellence in Materials Science and Technology, Chiang Mai University, Chiang Mai, 50200, Thailand*
[4] *Material & Chemical Characterisation Facility MC², University of Bath, Bath BA2 7AY, UK*
[5] *Department of Chemistry, Swansea University, College of Science, Grove Building, Singleton Park, Swansea SA2 8PP, UK*
[6] *School of Chemistry, University of Edinburgh, Joseph Black Building, West Mains Road, Edinburgh, Scotland EH9 3JJ, UK*
[7] *Department of Chemical Engineering and Biotechnology, University of Cambridge, Philippa Fawcett Drive, Cambridge, CB3 0AS, UK*
[8] *University of Liverpool, School of Engineering, Liverpool L69 3BX, UK*

To be submitted to Bioelectrochemistry

(Special Issue for the Zelechow Meeting SMBCS'2019)

Proofs to F. Marken (f.marken@bath.ac.uk)

Abstract

A novel indirect electrochemical sensor is presented for the measurement of a wide range of analytes including reducing (e.g. glucose, fructose) and non-reducing sugars (e.g. sucrose, trehalose). Its innovation relies on the use of a palladium film creating a two-compartment cell to separate the electrochemical and the photocatalytic processes. In this original way, the electrochemical detection is separated from the potential complex matrix of the analyte (i.e. colloids, salts, additives, etc). Hydrogen is generated in the photocatalytic compartment by a Pt@g-C_3N_4 photocatalyst embedded into a hydrogen capture material composed of a polymer of intrinsic microporosity (PIM-1). The immobilised photocatalyst is deposited onto a thin palladium membrane which allows rapid pure hydrogen diffusion which is them monitored by chronopotentiometry (zero current) response in the electrochemical compartment. The concept is demonstrated herein for the analysis of sugar content in commercial soft drinks. There is no requirement for the analyte to be conducting with electrolyte or buffered. In this way, samples (biological or not) can be simply monitored by their exposition to blue LED light, opening the door to exciting energy conversion and waste-to-energy applications.

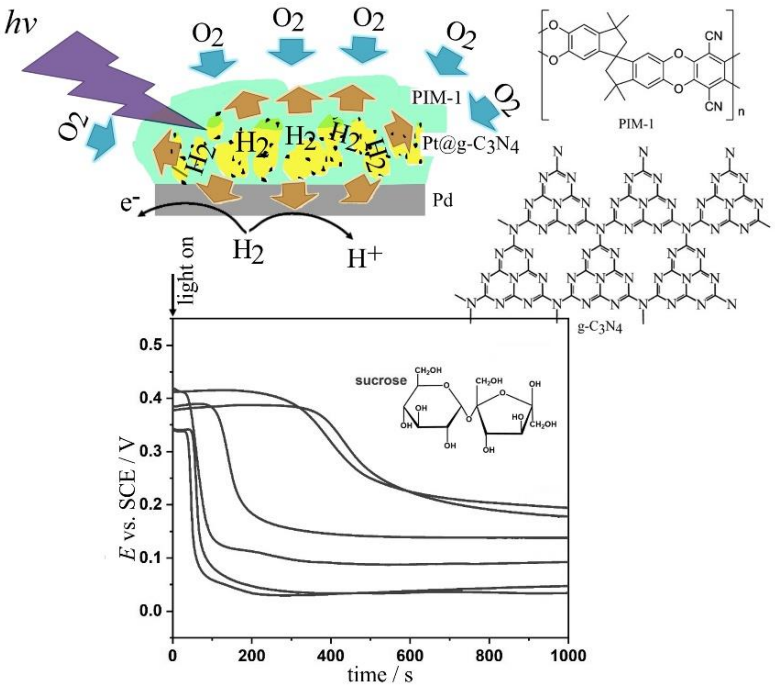

Graphical Abstract

Keywords: carbohydrate; hydrogen; photocatalysis; polymer; reaction layer; sensor

1. Introduction

Photo-electroanalytical sensing [1,2] and photo-bioelectroanalytical processes [3] provide a way to detect analytes under light-activated conditions with applied current/potential and illumination (continuous or pulsed [4 , 5]). There have been several cases of photo-electroanalytical procedures reported, for example for glucose detection [6], for miRNA [7], for mercury [8], and for ascorbate [9].

In this paper, a palladium film membrane cell is employed to separate the electrochemical compartment (see Figure 1) from the photo-catalysis compartment. This separation allows any type of analytical sample, independent of chemical nature or conductivity, to be studied without interference during the electrochemical detection. The palladium membrane purifies the hydrogen before detection and stops the direct interaction of sample and electrode. The process relies on the well-known Pt@g-C_3N_4 photocatalyst [10,11,12] and is based on a sequence of reaction steps. First, the excitation of Pt@g-C_3N_4 (equation 1) is followed by a charge separation step enhanced by the platinum deposit [13] (equation 2). Next, the hole can be captured either by water (to give oxygen, equation 3) or by a quencher such as glucose (to give oxidation products, equation 4). The remaining negative charge accumulates on the nano-platinum cocatalyst (here typically 2.5 nm diameter [14]), which results in the formation of hydrogen (equation 5) that then diffuses to/across the palladium membrane. After crossing the membrane, the electrochemical oxidation of hydrogen to protons (equation 6) is responsible for the establishment of a new equilibrium potential (in competition with reactions due to ambient oxygen). This sequence of reaction steps is oversimplified due to ambient oxygen introducing further complexity on both sides of the palladium membrane (*vide infra*).

$$Pt@g\text{-}C_3N_4 + h\nu \longrightarrow Pt@g\text{-}C_3N_4^* \quad (1)$$

$$Pt@g\text{-}C_3N_4^* \longrightarrow Pt^-@g\text{-}C_3N_4^+ \quad (2)$$

$$Pt^-@g\text{-}C_3N_4^+ + \tfrac{1}{2}\, H_2O \longrightarrow Pt^-@g\text{-}C_3N_4 + \tfrac{1}{2}\, O_2 + H^+ \quad (3)$$

$$Pt^-@g\text{-}C_3N_4^+ + \text{glucose} \longrightarrow Pt^-@g\text{-}C_3N_4 + \text{products} \quad (4)$$

$$Pt^{-}@g\text{-}C_3N_4 \quad + \quad H^{+} \longrightarrow \quad ½\ H_2(Pd) \qquad (5)$$

$$H_2(Pd) \longrightarrow \quad 2\ H^{+} \quad + \quad 2\ e^{-}(Pd) \qquad (6)$$

The immobilisation of the photocatalyst onto the palladium membrane surface can be achieved with a polymer of intrinsic microporosity. The use of a polymer of intrinsic microporosity (or PIM) is not only a simple scaffold to hold the catalyst without binding to the photocatalyst surface, but it is also beneficial, based on recent progress, in controlling the transport of gas molecules (under triphasic conditions) at electrode surfaces [15]. PIMs have been developed a decade ago [16] as a novel class of glassy (molecularly rigid) porous materials with excellent processability. Recently, these materials have emerged as useful components in electrochemical processes [17] due to the ability to stabilise surfaces, immobilise catalysts [18], and to capture gases such as hydrogen under "triphasic" conditions in the presence of aqueous electrolytes [19]. PIM-1 offers a surface area (BET) of typically 750 m^2g^{-1} [20] and pores of around 1-2 nm [21].

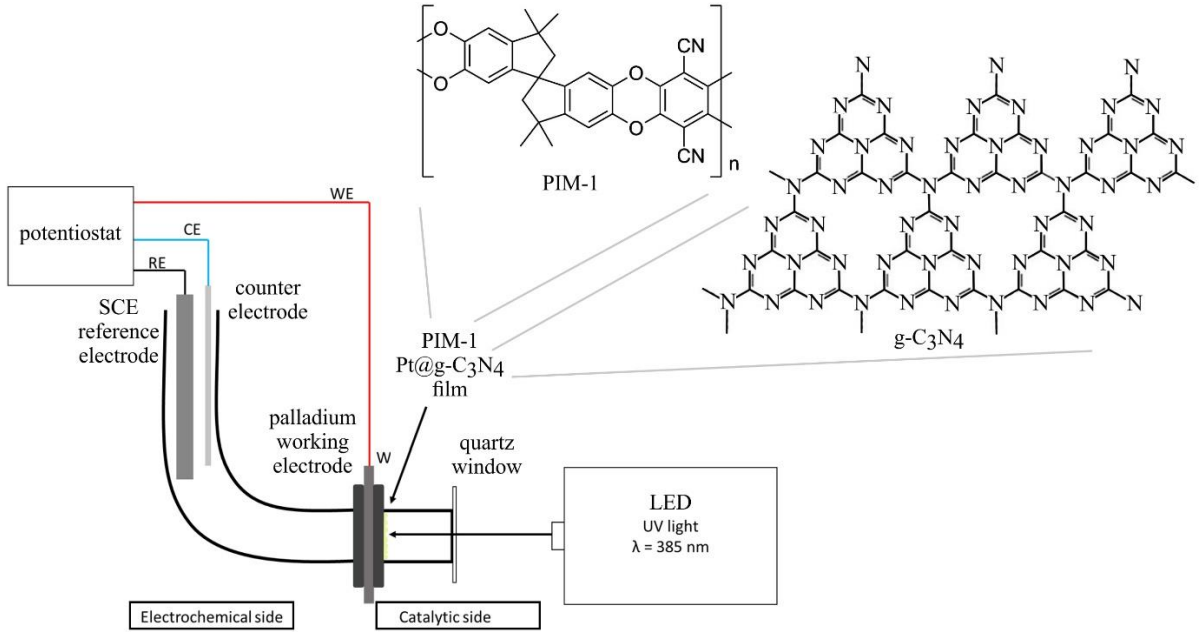

Figure 1. Schematic illustration of an experimental system with a palladium film (25 μm thickness; optically dense), an electrochemical compartment with counter, reference, and working electrode immersed in aqueous 10 mM HCl, and a photo-catalysis compartment (where analyte is placed) with quartz window, optical path length 15 mm, 385 nm wave length, approximately 100 $mWcm^{-2}$ LED light source.

In this paper, novel exploratory data are presented to demonstrate the concept of an "indirect" carbohydrate sensor, based on an indirect electrochemical process (*via* palladium membrane) and driven by blue light (λ = 385 nm) in a photo-catalytic reaction. The Pt@g-C_3N_4 photocatalyst is employed in conjunction with the hydrogen capturing PIM-1 polymer of intrinsic microporosity. Different types of carbohydrates (reducing and non-reducing) are shown to produce detectable photoresponses. Potential for application of "indirect sensing" is demonstrated with commercial softdrinks.

2. Experimental

2.1. Reagents

All chemicals were purchased from Sigma-Aldrich and used without any further purification. Palladium membrane (0.025 mm thickness, 99.95 % purity, light tested) was bought from Goodfellow Ltd. PIM-1 was prepared following a literature procedure [22]. Commercial softdrinks (a glucose-containing softdrink "Innocent Coconut Water" (Innocent UK) and a sweetener-containing softdrink "Oasis Aquashock Chilled Cherry" (Coca Cola UK)) were bought from a local supermarket. Deionized water (18.2 MΩ cm at 20 ^{o}C obtained from a CE Instruments Ltd. water purification system) was used to prepare electrolyte solutions. All experiments are conducted in an ambient environment (T = 22 ± 2 ^{o}C).

2.2. Instrumentation

Electrochemical measurements were conducted with a potentiostat system (μAUTOLAB III, Metrohm, Herisau, Switzerland). GPES software was used to record the data. A KCl-saturated calomel electrode (SCE) was used as the reference electrode together with a platinum wire as the counter electrode. Transmission electron microscopy (TEM) images for Pt@g-C_3N_4 materials were captured with a JEOL JSM-2010Plus (JEOL U.K. Ltd, Welwyn Garden City, UK). An LED light source wavelength 385 nm was employed (Thorlabs, Inc., M385LP1). ^{1}H NMR spectra was recorded on a Bruker 500 MHz spectrometer. Mass spectrometry analyses were performed on an Automated Agilent QTOF (Walkup) used with HPLC (4 chromatography columns) and variable wavelength detector (VWD). LC-MS analyses were performed using an Agilent QTOF 6545 with Jetstream ESI spray source coupled to an Agilent

1260 Infinity II Quat pump HPLC with 1260 autosampler, column oven compartment and variable wavelength detector (VWD).

2.3. Procedures

Synthesis of Pt@g-C_3N_4. First, melamine (Sigma-Aldrich, 99 % purity) was added into a ceramic boat with lid, which was then placed into the centre of an Elite horizontal tube furnace (TSH12/65/550) and heated to 500 °C for three hours. After cooling overnight, the final g-C_3N_4 was obtained as pale yellow powder. Next, potassium hexachloroplatinate(IV) (K_2PtCl_6) (purchased from Sigma-Aldrich, >99.9 % purity) (40 mg) and 0.4 g of the synthesised g-C_3N_4 were added into 25 mL of saturated sodium oxalate solution in a glass vial. In order to deposit platinum nanoparticles (Pt^0) onto the g-C_3N_4, the reaction mixture was irradiated with blue light (λ = 385 nm) for 60 hours with continuous stirring. Pt@g-C_3N_4 catalyst was finally separated and collected by centrifuging, washing, and drying in an oven.

Immobilisation of photocatalyst into PIM-1. Pt@g-C_3N_4 catalyst was dispersed together with the polymer of intrinsic microporosity (PIM-1) in a chloroform solution. The mixture was ultrasonicated in a water bath for 15 mins before use. Deposits were formed by drop-casting.

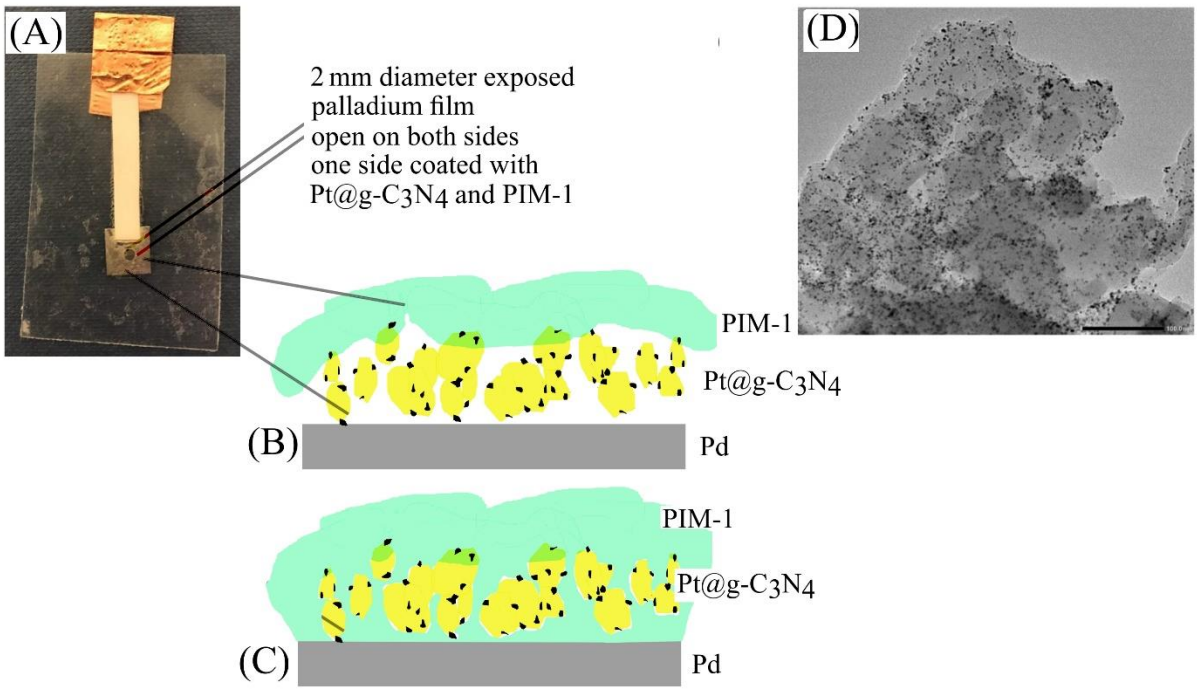

Figure 2. (A) Photograph of the laminated palladium film exposed with 2 mm diameter holes on both sides. (B) Schematic drawing of Pt@g-C_3N_4 immobilised on palladium and coated with PIM-1. (C) Schematic drawing of Pt@g-C_3N_4 with PIM-1 coated as a single layer. (D) Typical transmission electron micrograph (TEM) for Pt@g-C_3N_4.

Preparation of Pd membrane. A piece of commercial document lamination foil was firstly punctured with a hole with a 2 mm diameter. A Pd foil (0.025 mm thickness, 0.5 cm × 0.5 cm, Goodfellow Ltd.) was then placed between the two pieces of the laminate (see Figure 2A). A strip of copper film was placed in contact with the Pd foil for electrical connection. The laminate was then sealed with a hot iron to achieve sealing. Figure 2B and 2C show schematic drawings of the photocatalyst deposited with a PIM-1 coating and a mixed coating with both photocatalyst and PIM-1. The latter proved to be a more robust methodology and was applied throughout the study. In Figure 2D TEM images are shown revealing platinum nanoparticles of typically 2.5 nm diameter.

3. Results and Discussion

3.1. Pt@g-C_3N_4 Photopotential Responses due to Hydrogen from Glucose

The production of hydrogen from glucose by the Pt@g-C_3N_4 photocatalyst can be revealed due to rapid hydrogen diffusion through the adjacent palladium film [23]. The diffusion coefficient for hydrogen in palladium has been reported as approximately 10^{-11} m^2s^{-1} at room temperature [24] and therefore the response time delay due to hydrogen diffusing through the L = 25 μm membrane will be typically $\tau \approx L^2/D$ = 60 s. The advantage of the palladium film separating the electrochemical compartment and the photocatalysis compartment (see Figure 1) is based on the purification of the hydrogen transiting the palladium. In this way it is possible to suppress any interfering redox response from the sample.

Chronoamperometry at zero current was chosen to follow the photoresponse in terms of an equilibrium potential signal. Figure 4A shows some typical chronoamperometry data traces. Only distilled water (i) does not lead to a significant potential response due to oxygen on both sides of the palladium membrane dominating the redox equilibrium. Trace (ii) shows a slight

negative shift, but with a stable equilibrium potential when 0.1 M NaOH is added into the catalysis compartment. The presence of glucose in the aqueous solution makes a significant difference. In both, water with glucose (iii) and 0.1 M NaOH with glucose (iv), a delayed and pronounced shift to negative potentials (0.00 and -0.12 V vs. SCE, respectively) is observed. This shift can be attributed to the photocatalytic hydrogen evolution due to glucose acting as a hole quencher. Perhaps interestingly, the delay is more pronounced in 0.1 M NaOH, but the final potential is also substantially more negative (more hydrogen is produced). The delay is (at least in part) due to the need to locally consume oxygen present on both sides of the palladium membrane (*vide infra*). Due to the complexity of the chemistry of glucose in alkaline media and the additional benefit of not requiring any electrolyte in the photocatalysis compartment, the following experiments were conducted in pure water.

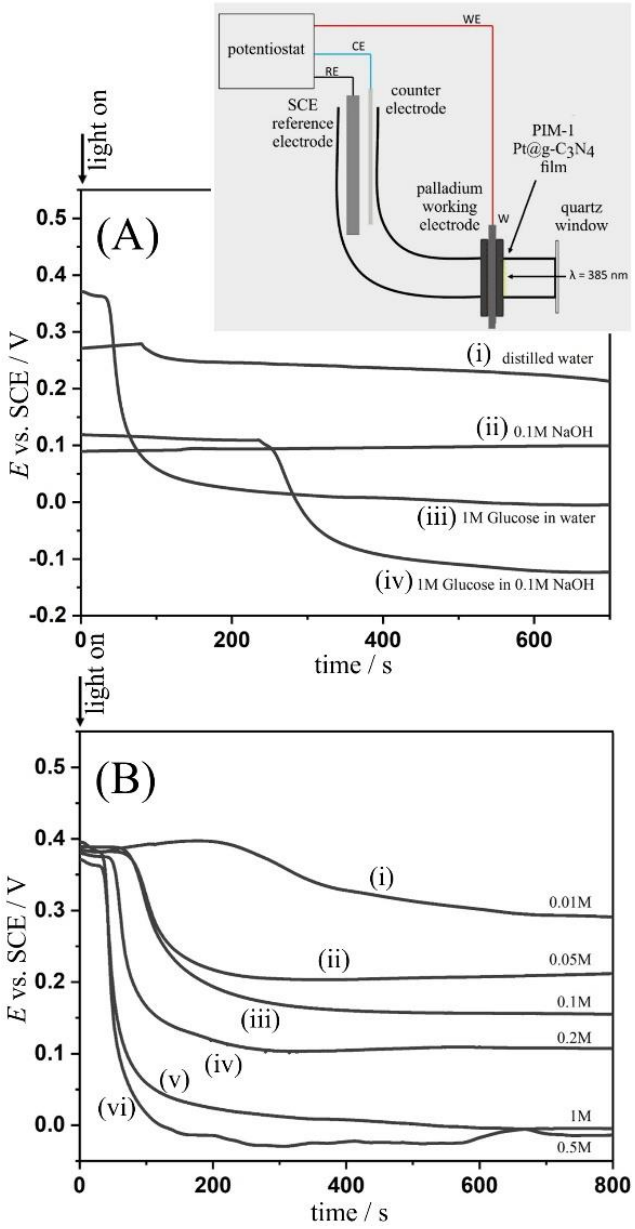

Figure 3. (A) Chronopotentiometry (zero current) for a palladium film in contact to four different solutions: (i) distilled water, (ii) 0.1 M NaOH, (iii) 1M glucose in water, and (iv) 1 M glucose in 0.1 M NaOH. Photocatalyst: 60 µg Pt@g-C_3N_4 mixed with 12 µg PIM-1 on a 2 mm diameter Pd membrane area. At time zero the LED is switched on. Electrochemical compartment (see inset) with aqueous 10 mM HCl. (B) Chronoamperometry (zero current) for glucose in water with (i) 0.01, (ii) 0.05, (iii) 0.1, (iv) 0.2, (v) 0.5, and (vi) 1 M glucose.

Data in Figure 3B were obtained with different concentrations of glucose dissolved in water. An amount of 60 µg Pt@g-C_3N_4 photocatalyst was immobilsied together with 12 µg PIM-1. A signal can be measured for a concentration as low as 10 mM glucose. However, the delay is substantial (300 s) and the final potential does not significantly shift. When increasing the glucose concentration, the hydrogen response is observed to be faster (within 60 s) and the shift

in equlibrium potentail is more pronounced. A dependence of the final equilibrium potential on the glucose concentration is observed.

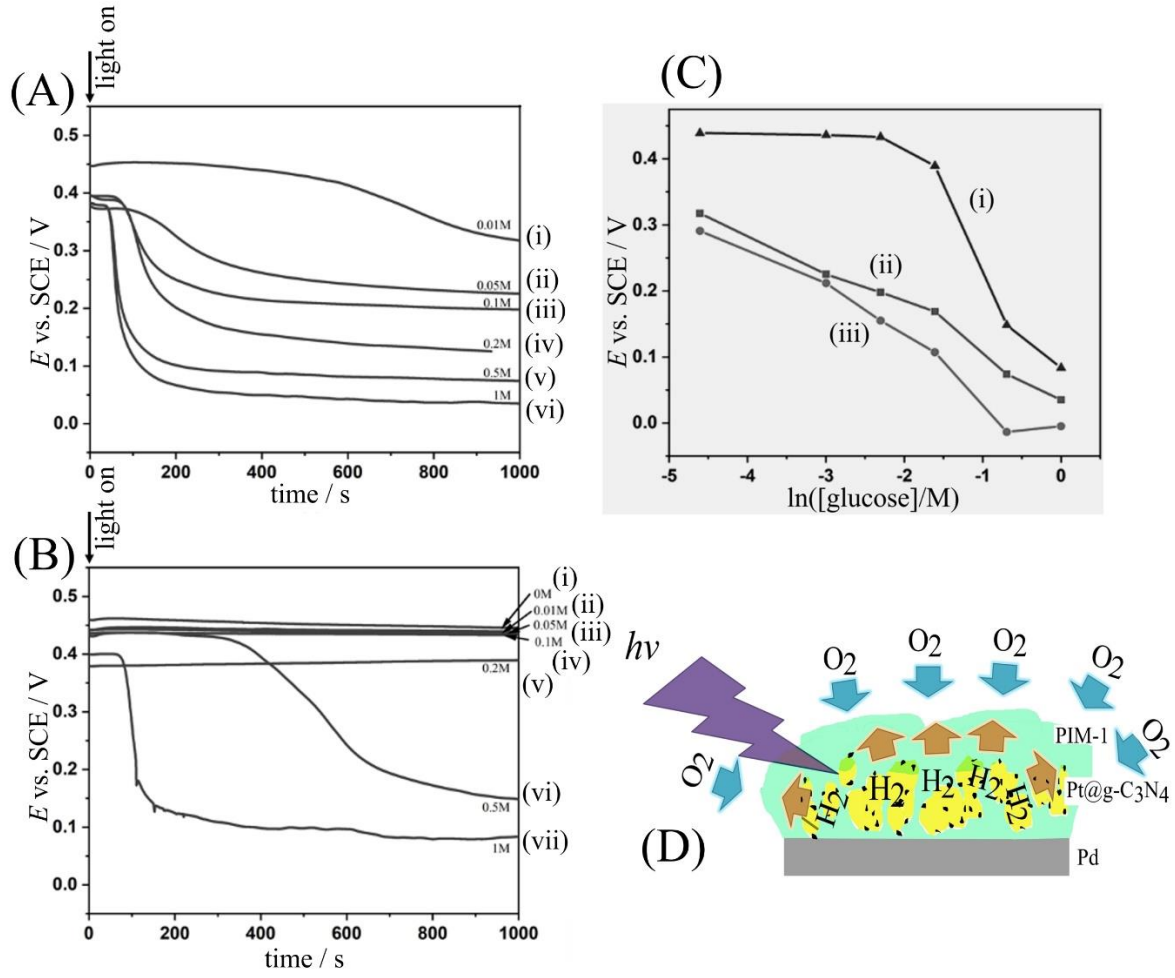

Figure 4. (A) Chronopotentiometry (zero current) with 60 μg Pt@g-C_3N_4 and 24 μg PIM-1 on palladium in (i) 0.01, (ii) 0.05, (iii) 0.1, (iv) 0.2, (v) 0.5, and (vi) 1 M glucose in water. (B) As before but for only 60 μg Pt@g-C_3N_4 and no PIM-1. (C) Summary plot of end potential (at 1000 s) as a function of glucose concentration in water for (i) no PIM-1, (ii) 24 μg PIM-1, and (iii) 12 μg PIM-1. (D) Schematic drawing of the photocatalytic hydrogen production under a PIM-1 film competing with oxygen ingress.

Next, the effect of the PIM-1 polymer is investigated. Figure 4 shows chronoamperometry (zero current) data obtained for (A) 60 μg Pt@g-C_3N_4 with 24 μg PIM-1 and (B) 60 μg Pt@g-C_3N_4 with no PIM-1. The presence of the polymer of intrinsic microporosity does affect the behavour of the photocatalyst. An increase in PIM-1 appears to slow down the photoresponse as well as shifting the final equlibrium potential slightly more positive. This increase and shift

is consistent with the additional PIM-1 either slowing diffusional access to the photocatalyst or somewhat lowering the light intensity at the location of the photocatalyst.

In the absence of PIM-1 (see Figure 4B), the equilibrium potential response is significantly delayed and observed only for very high concentrations of glucose (for less than 0.5 M glucose the process occurs not within 1000 s). This can be explained with the competing fluxes of hydrogen and oxygen to the photocatalyst. Figure 4D shows a schematic diagram indicating production of hydrogen at the photocatalyst and diffusion of oxygen from outside into the PIM-1 layer. As a microporous polymer, PIM-1 is open to small molecule diffusion, e.g. glucose, protons, water, and to gas diffusion, e.g. hydrogen and oxygen. However, under triphasic conditions transport of oxygen may be slowed down during hydrogen production. Therefore, the PIM-1 material not only provide mechanical stabilisation of the Pt@g-C_3N_4 photocatalyst, but also a protection against oxygen improving the flux of hydrogen into the palladium membrane. The optimum effects are observed with 60 μg Pt@g-C_3N_4 and 12 μg PIM-1.

Data plotted in Figure 4C shows the effect of PIM-1 when equilibrium potential data is plotted versus glucose concentration. Without PIM-1 present a delayed and dramatic change is observed. With the PIM-1 present, a more gradual change occurs, and this could be useful when analytically detecting glucose or other types of carbohydrates.

3.2. Pt@g-C_3N_4 Photopotential Responses due to Hydrogen Produced from Different Carbohydrates

The effects of the carbohydrate molecular structure on the photoresponse was investigated, in particular in view of the behaviour of reducing versus non-reducing sugars. Figure 5 shows chronoamperometry (zero current) data for glucose, fructose (reducing) as well as sucrose and trehalose (non-reducing). It is clear that both reducing and non-reducing sugars give significant photoresponses. It has previously been suggested that the reaction of the sugar is likely to be associated with its adsorption onto the g-C_3N_4 photocatalyst [14] and therefore holes of high energy (2.7 eV band gap [25]) may be sufficiently energetic to trigger oxidation even for non-reducing carbohydrates. For trehalose (Figure 5A), the photoresponse is delayed and observed only for concentrations higher than 0.1 M. However, for sucrose (Figure 5B) only a weak

delayed signal is observed. Both glucose (Figure 3B) and fructose (Figure 5C) show photoresponses over the complete concentration range. The plot in Figure 5D summarises and compares the final equilibrium potential data (at 1000 s) for the four types of carbohydrate.

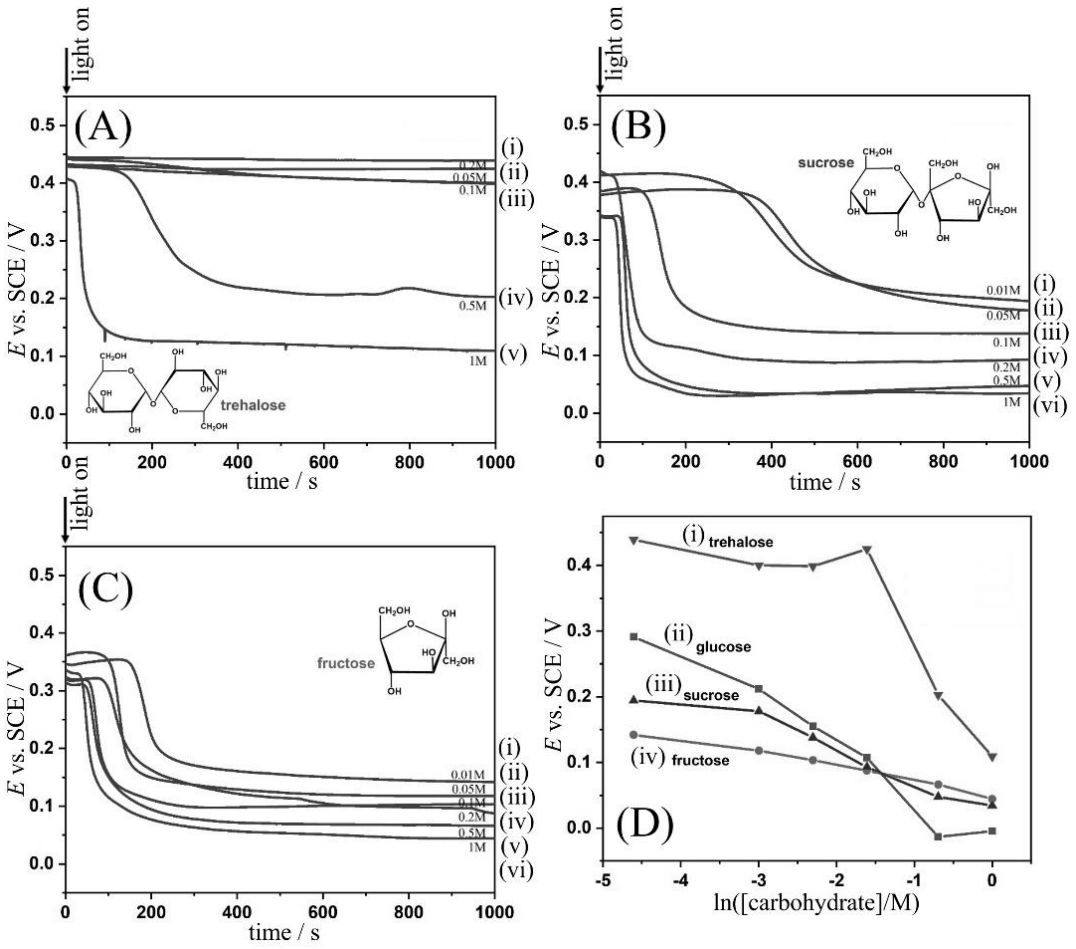

Figure 5. (A) Chronopotentiometry (zero current) data obtained with 60 μg Pt@g-C_3N_4 and 12 μg PIM-1 at a palladium membrane for (i) 0.05, (ii) 0.1, (iii) 0.2, (iv) 0.5, and (v) 1 M trehalose in water. (B) As above but for sucrose. (C) As above but for fructose. (D) Plot of the final equilibrium potential (at 1000 s) versus carbohydrate concentration in water for (i) trehalose, (ii) glucose, (iii) sucrose, and (iv) fructose.

3.3. Pt@g-C_3N_4 Photopotential Responses due to Hydrogen Generation from Soft Drink Samples

A potential area of application of the photopotential generation for carbohydrates could be in monitoring of commercial products containing sugars. The palladium membrane is dense separating the electrochemical compartment from the photocatalysis compartment. Complex samples of any type (even in oils etc.) could be in contact and used to generate photoresponses.

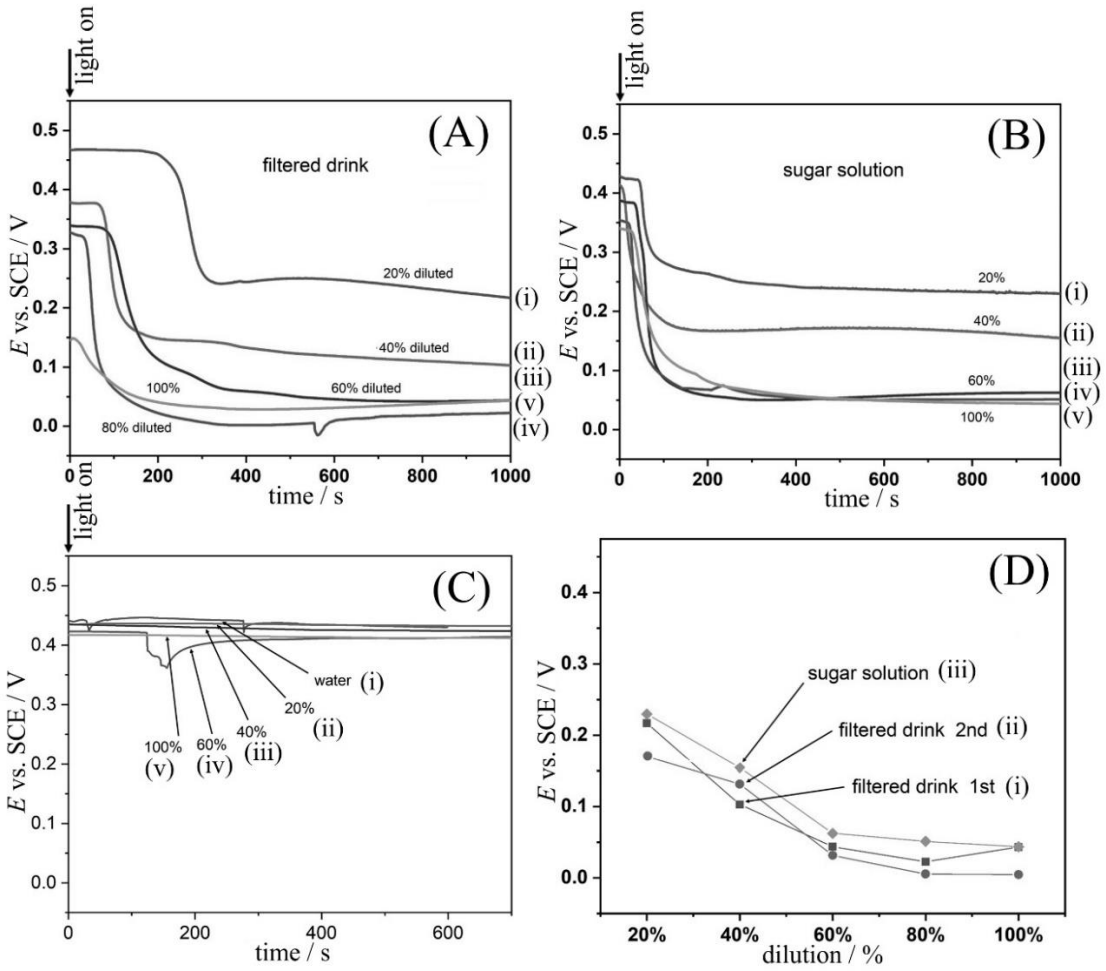

Figure 6. (A) Chronopotentiometry (zero current) data for 60 µg Pt@g-C_3N_4 and 12 µg PIM-1 at a palladium membrane obtained for a filtered commercial soft drink containing a mixture of carbohydrates as a function of dilution. (B) As before, but for an aqueous solution of glucose : fructose : sucrose with molar ratio 1 : 4.95 : 2.42 and with total content of 0.35 g glucose + 1.75 g fructose + 1.30 g sucrose in 100 mL water to mimic the soft drink. (C) As before but for a filtered soft drink with artificial sweetener. (D) Plot of final equilibrium potential data (at 1000 s) for (i) the filtered drink, (ii) a repeat measurement for the filtered drink, and (iii) the artificial sugar solution as a function of dilution.

Here, commercial softdrink samples were purchased and tested. Figure 6A shows the photoresponse for a sugar containing softdrink (see experimental). Filtration was necessary as turbidity affected the measurement. However, in future this could be avoided by shortening the optical path length (here 15 mm). By diluting the sample systematically, a set of data points

was recorded. NMR analysis of the product (see supporting information) revealed the presence of an aqueous glucose : fructose : sucrose solution with molar ratio 1 : 4.95 : 2.42 and with total content of 0.355 g glucose + 1.75 g fructose + 1.3 g sucrose in 100 mL water. An artificial solution of identical composition was used for comparison purposes. Data in Figure 6B show very similar photoresponses upon dilution. A softdrink with sweetener (no carbohydrates) did not give any significant photoresponse (Figure 6C). The plot in Figure 6D shows data for two repeat data sets of the sugar-containing softdrink together with the data for the artificial mixture of sugars showing a good agreement.

It should be noted that these measurements were all performed in the presence of ambient oxygen and this affects the equilibrium potential data (as oxygen will react with hydrogen at the palladium surface). Additional experiments (not shown) with argon de-aeration cause a shift of the final equilibrium to more negative potentials. Argon de-aeration only on the sample side does not speed up the photoresponse, but results in a shift in final potential by approximately -50 mV. However, when argon de-aerating both sides of the palladium membrane, the final equilibrium potential with the softdrink approaches -0.2 V vs. SCE. Therefore, the conditions (oxygen content) on both sides of the palladium membrane during the analytical detection are important. Applications of this methodology seem most plausible for approximation/monitoring of total carbohydrate content in the presence of ambient oxygen. In future, improvements in the analytical performance are likely for example with thinner palladium composite membranes, with photo-chronoamperometric techniques, or based on voltammetric read-out of photocurrents.

4. Conclusions

It has been shown that a palladium film can be employed to separate an analyte compartment with glucose and an electrochemical compartment filled with aqueous 10 mM HCl. Production of hydrogen in the analyte compartment driven by a blue LED (385 nm) and catalysed by a Pt@g-C_3N_4 photocatalyst deposit causes the equilibrium potential of the palladium working electrode to respond. A PIM-1 matrix for the Pt@g-C_3N_4 photocatalyst was employed to help capturing the hydrogen, protect against oxygen, and to provide a mechanically stable catalyst film.

When glucose was introduced as a hole quencher, significant photo-responses are recorded as change in equilibrium potential. The process is effective in distilled water, in commercial softdrink, or fruit juice samples. The measurable glucose concentrations range appeared to be from about 10 mM to approximately 300 mM in the presence of ambient oxygen. However, other types of carbohydrates such as fructose (reducing), or sucrose, trehalose (non-reducing) give photoresponses with similar characteristics. For commercial samples only the total content for a given mixtures of carbohydrates is measured. Distinguishing between the different types of quenchers is not possible under these conditions.

The "indirect electrochemical sensor" methodology is novel in that the separation of electrochemical and analysis compartments allows the electrochemical detection to be separated from complex matrix elements (colloids, salts, additives, etc.). There is no requirement for the analyte to be conducting with electrolyte or buffered. Samples (biological or non-biological) can be monitored simply in contact to the membrane and exposed to blue light from an LED light source. In the future, a wider range of applications may be possible. However, the sensitivity as well as the response time of the sensor need to be improved for example by introducing much thinner types of membranes. Further applications beyond sensor development are possible in energy conversion and in waste-to-energy applications.

Acknowledgements

Y.Z. thanks the China Scholarship Council (CSC scholarship No 20180935006) for a PhD scholarship. E.M., L.T.M., K.B., and F.M. thank EPSRC for support (EP/N013778/1).

References

[1] L. Shi, Y. Yin, L.C. Zhang, S.B. Wang, M. Sillanpää, H.Q. Sun, Design and engineering heterojunctions for the photoelectrochemical monitoring of environmental pollutants: A review, Appl. Catal. B-Environmental 248 (2019) 405–422.

[2] B. Sun, S.Y. Ai, Fabrication and application of photoelectrochemical sensor, Progress Chem. 26 (2014) 834–845.

[3] L.T. Wey, P. Bombelli, X.L. Chen, J.M. Lawrence, C.M. Rabideau, S.J.L. Rowden, J.Z. Zhang, C.J. Howe, The development of biophotovoltaic systems for power generation and biological analysis, ChemElectroChem (2019) DOI: 10.1002/celc.201900997.

[4] F.W.P. Ribeiro, F.C. Moraes, E.C. Pereira, F. Marken, L.H. Mascaro, New application for the $BiVO_4$ photoanode: A photoelectroanalytical sensor for nitrite, Electrochem. Commun. 61 (2015) 1–4.

[5] S.Y. Yu, L. Zhang, L.B. Zhu, Y. Gao, G.C. Fan, D.M. Han, G.X. Chen, W.W. Zhao, Bismuth-containing semiconductors for photoelectrochemical sensing and biosensing, Coordination Chem. Rev. 393 (2019) 9–20.

[6] B. Cakiroglu, M. Ozacar, A self-powered photoelectrochemical glucose biosensor based on supercapacitor Co_3O_4-CNT hybrid on TiO_2, Biosens. Bioelectronics, 119 (2018) 34–41.

[7] N.N. Fu, Y. Hu, S.H. Shi, S.K. Ren, W. Liu, S. Su, B.M. Zhao, L.X. Weng, L.H. Wang, Au nanoparticles on two-dimensional MoS_2 nanosheets as a photoanode for efficient photoelectrochemical miRNA detection, Analyst, 143 (2018) 1705–1712.

[8] N.N. Xu, T. Hou, F. Li, A label-free photoelectrochemical aptasensor for facile and ultrasensitive mercury ion assay based on a solution-phase photoactive probe and exonuclease III-assisted amplification, Analyst, 144 (2019) 3800–3806.

[9] J.A. Cooper, K.E. Woodhouse, A.M. Chippindale, R.G. Compton, Photoelectrochemical determination of ascorbic acid using methylene blue immobilized in alpha-zirconium phosphate, Electroanalysis, 11 (1999) 1259–1265.

[10] G.P. Dong, Y.H. Zhang, Q.W. Pan, J.R. Qiu, A fantastic graphitic carbon nitride (g-C_3N_4) material: Electronic structure, photocatalytic and photoelectronic properties, J. Photochem. Photobiol. C-Photochem. Rev. 20 (2014) 33–50.

[11] F. Fina, H. Menard, J.T.S. Irvine, The effect of Pt NPs crystallinity and distribution on the photocatalytic activity of Pt-g-C_3N_4, Phys. Chem. Chem. Phys. 17 (2015) 13929–13936.

[12] Y. Zheng, L.H. Lin, B. Wang, X.C. Wang, Graphitic carbon nitride polymers toward sustainable photoredox catalysis, Angew. Chem. Inter. Ed. 54 (2015) 12868–12884.

[13] J.Q. Wen, J. Xie, X.B. Chen, X. Li, A review on g-C_3N_4-based photocatalysts, Appl. Surf. Sci. 391 (2017) 72–123.

[14] Y.Z. Zhao, N.A. Al Abass, R. Malpass-Evans, M. Carta, N.B. McKeown, E. Madrid, P.J. Fletcher, F. Marken, Photoelectrochemistry of immobilised Pt@g-C_3N_4 mediated by hydrogen and enhanced by a polymer of intrinsic microporosity PIM-1, Electrochem. Commun. 103 (2019) 1–6.

[15] F. Marken, E. Madrid, Y.Z. Zhao, M. Carta, N.B. McKeown, Polymers of intrinsic microporosity in triphasic electrochemistry: perspectives, ChemElectroChem 6 (2019) 4332–4342.

[16] N.B. McKeown, P.M. Budd, Exploitation of intrinsic microporosity in polymer-based materials, Macromolecules, 43 (2010) 5163–5176.

[17] E. Madrid, N.B. McKeown, Innovative methods in electrochemistry based on polymers of intrinsic microporosity, Curr. Opinion Electrochem. 10 (2018) 61–66.

[18] D.P. He, D.S. He, J.L. Yang, Z.X. Low, R. Malpass-Evans, M. Carta, N.B. McKeown, F. Marken, Molecularly rigid microporous polyamine captures and stabilizes conducting platinum nanoparticle networks, ACS Appl. Mater. Interfaces 8 (2016) 22425–22430.

[19] E. Madrid, J.P. Lowe, K.J. Msayib, N.B. McKeown, Q.L. Song, G.A. Attard, T. Düren, F. Marken, Triphasic nature of polymers of intrinsic microporosity induces storage and catalysis effects in hydrogen and oxygen reactivity at electrode surfaces, ChemElectroChem 6 (2019) 252–259.

[20] H.R. Kricheldorf, D. Fritsch, L. Vakhtangishvili, N. Lomadze, G. Schwarz, Cyclic ladder polymers based on 5,5 ', 6,6 '-tetrahydroxy-3,3,3 ', 3 '-tetramethylspirobisindane and 2,3,5,6-tetrafluoropyridines, Macromolecules 39 (2006) 4990–4998.

[21] G.S. Larsen, P. Lin, K.E. Hart, C.M. Colina, Molecular simulations of PIM-1-like polymers of intrinsic microporosity, Macromolecules 44 (2011) 6944–6951.

[22] P.M. Budd, E.S. Elabas, B.S. Ghanem, S. Makhseed, N.B. McKeown, K.J. Msayib, C.E. Tattershall, D. Wang, Solution-processed, organophilic membrane derived from a polymer of intrinsic microporosity, Adv. Mater. 16 (2004) 456–459.

[23] R.S. Sherbo, R.S. Delima, V.A. Chiykowski, B.P. MacLeod, C.P. Berlinguette, Complete electron economy by pairing electrolysis with hydrogenation, Nature Catalysis 1 (2018) 501–507.

[24] R.V. Bucur, The influence of experimental conditions upon the measurements of hydrogen diffusion in palladium be electrochemical permeation methods, Zeitschrift Physikalische Chemie Neue Folge 146 (1985) 217–229.

[25] A. Naseri, M. Samadi, A. Pourjavadi, A.Z. Moshfegh, S. Ramakrishna, Graphitic carbon nitride (g-C_3N_4)-based photocatalysts for solar hydrogen generation: recent advances and future development directions, J. Mater. Chem. A 5 (2017) 23406–23433.

Supporting Information

Indirect Photo-Electrochemical Detection of Carbohydrates with Pt@g-C_3N_4 Immobilised into a Polymer of Intrinsic Microporosity (PIM-1) and Attached to a Palladium Hydrogen Capture Membrane

Yuanzhu Zhao [1], Joshua Dobson [1], Catajina Harabajiu [1], Elena Madrid [1], Tinakorn Kanyanee [1,2,3], Catherine Lyall [1,4], Shaun Reeksting [1,4], Mariolino Carta [5], Neil B. McKeown [6], Laura Torrente-Murciano [7], Kate Black [8], and Frank Marken [1]*

[1] *Department of Chemistry, University of Bath, Claverton Down, Bath BA2 7AY, UK*
[2] *Department of Chemistry, Faculty of Science, Chiang Mai University, Chiang Mai, 50200, Thailand*
[3] *Center of Excellence in Materials Science and Technology, Chiang Mai University, Chiang Mai, 50200, Thailand*
[4] *Material & Chemical Characterisation Facility MC[2], University of Bath, Bath BA2 7AY, UK*
[5] *Department of Chemistry, Swansea University, College of Science, Grove Building, Singleton Park, Swansea SA2 8PP, UK*
[6] *School of Chemistry, University of Edinburgh, Joseph Black Building, West Mains Road, Edinburgh, Scotland EH9 3JJ, UK*
[7] *Department of Chemical Engineering and Biotechnology, Cambridge University, Cambridge, CB3 0AS, UK*
[8] *University of Liverpool, School of Engineering, Liverpool L69 3BX, UK*

Content

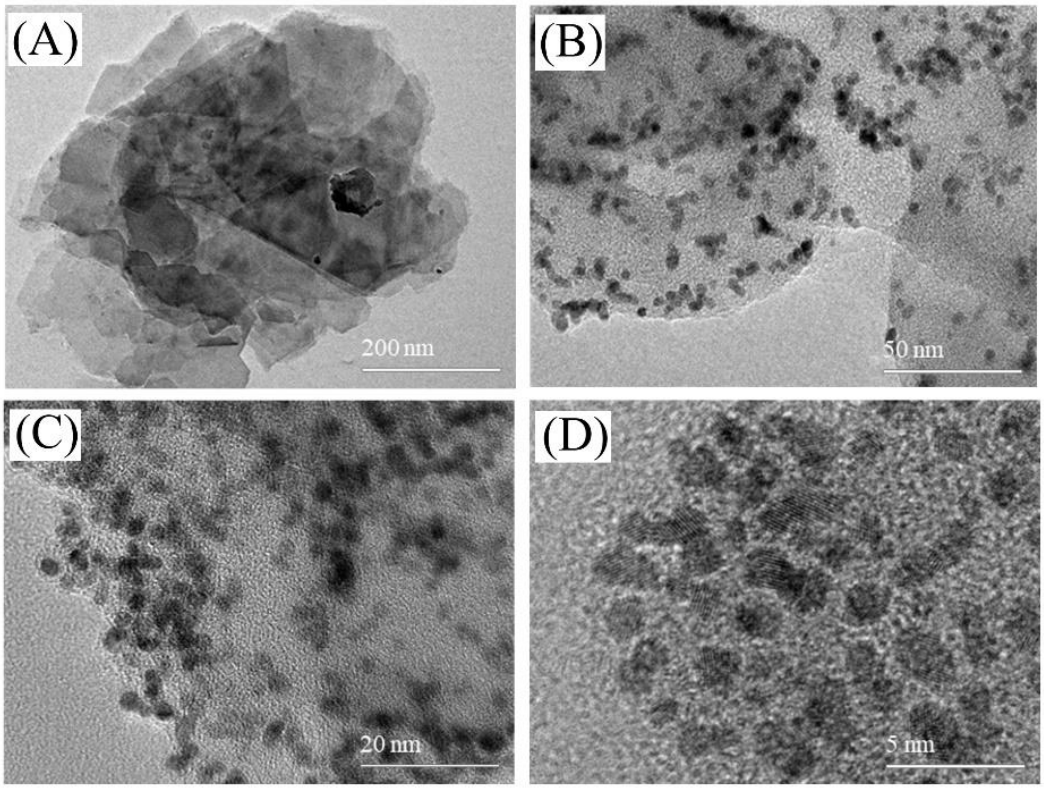

Figure S1. TEM images of (A) g-C_3N_4; (B)-(D) g-C_3N_4 with Pt nanoparticles deposition.

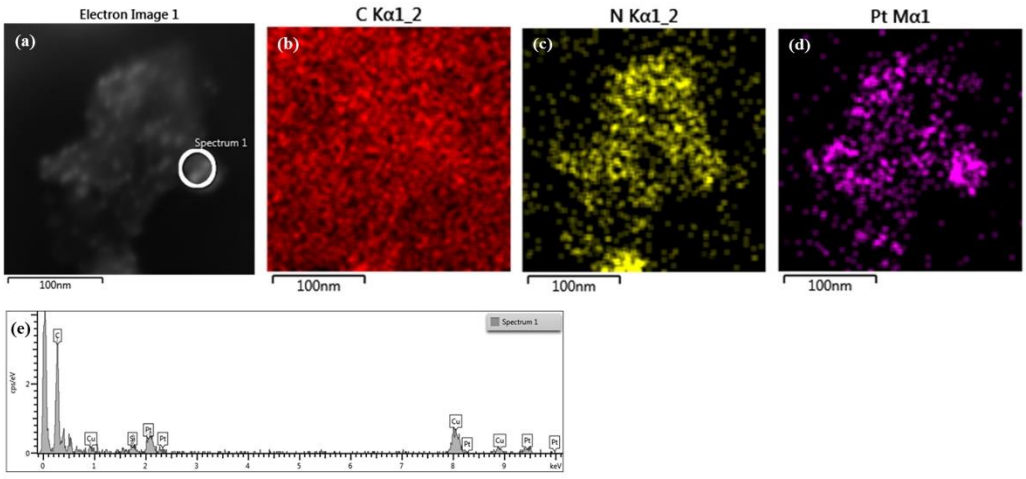

Figure S2. Element mapping of the Pt@g-C_3N_4 (a) the sample; (b)-(d) exhibit of element of carbon, nitrogen and platinum; (e) EDS spectrum.

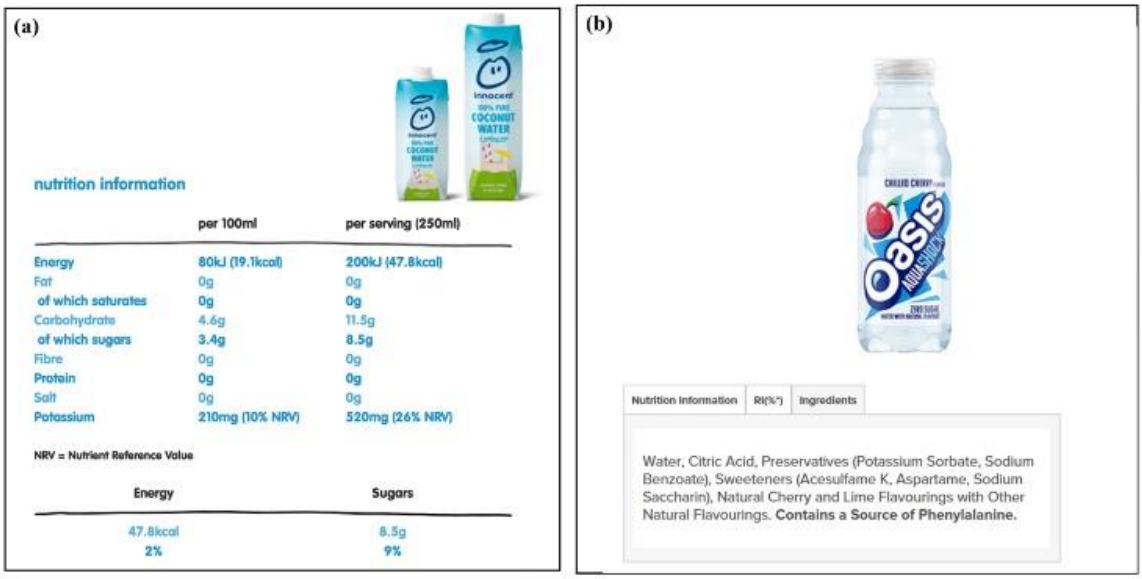

Figure S3. Nutritional information about softdrinks used in sugar sensing experiments: (a) sugar-containing Innocent Coconut Water (Innocent Company); (b) non-sugar containing softdrink Oasis Zero (Coca Cola Company). Information source: https://www.innocentdrinks.co.uk/things-we-make/coconut-water; https://www.coca-cola.co.uk/drinks/oasis-aquashock/oasis-aquashock-chilled-cherry.

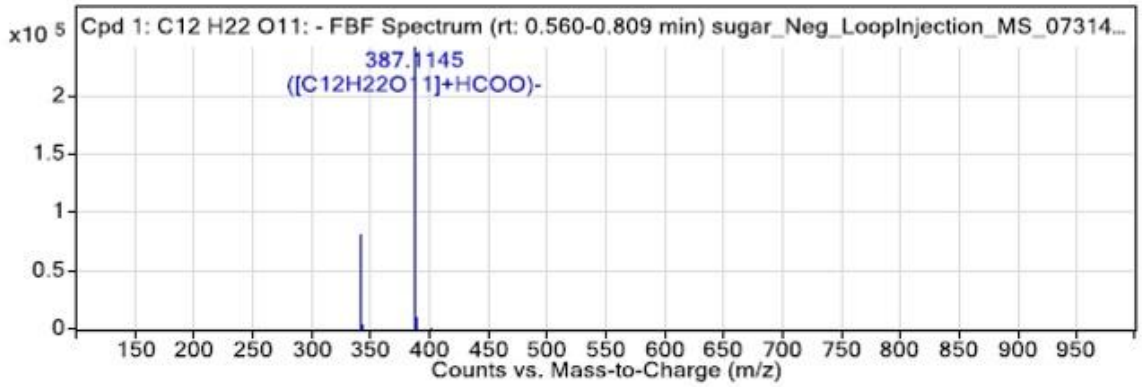

Peak List

m/z	z	Abund	Formula	Ion
341.1087	1	79390.41	C12H22O11	(M-H)-
342.112	1	10842.7	C12H22O11	(M-H)-
343.1181	1	3201.68	C12H22O11	(M-H)-
387.1145	1	240391.2	C12H22O11	(M+HCOO)-
388.1176	1	37053.39	C12H22O11	(M+HCOO)-
389.1206	1	9313.35	C12H22O11	(M+HCOO)-
401.1404	1	201.17	C12H22O11	(M+CH3COO)-

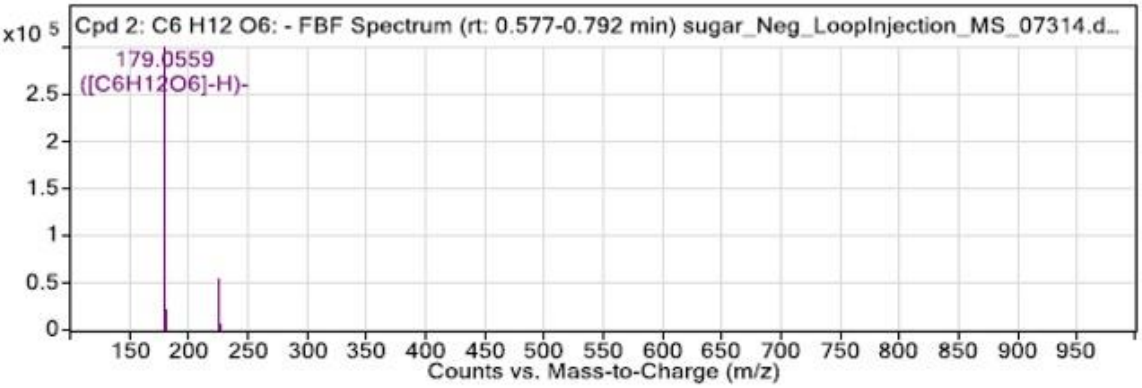

Peak List

m/z	z	Abund	Formula	Ion
179.0559	1	300229.84	C6H12O6	(M-H)-
180.0591	1	20382.44	C6H12O6	(M-H)-
225.0611	1	53321.3	C6H12O6	(M+HCOO)-
226.0644	1	4694.64	C6H12O6	(M+HCOO)-

Figure S4. Mass spectrometry data for the sugar containing softdrink. All three, sucrose ($C_{12}H_{22}O_{11}$) and glucose/fructose ($C_6H_{12}O_6$) could be detected with negative mode ionization using loop injection within 5 ppm mass error from the mass spectrometry.

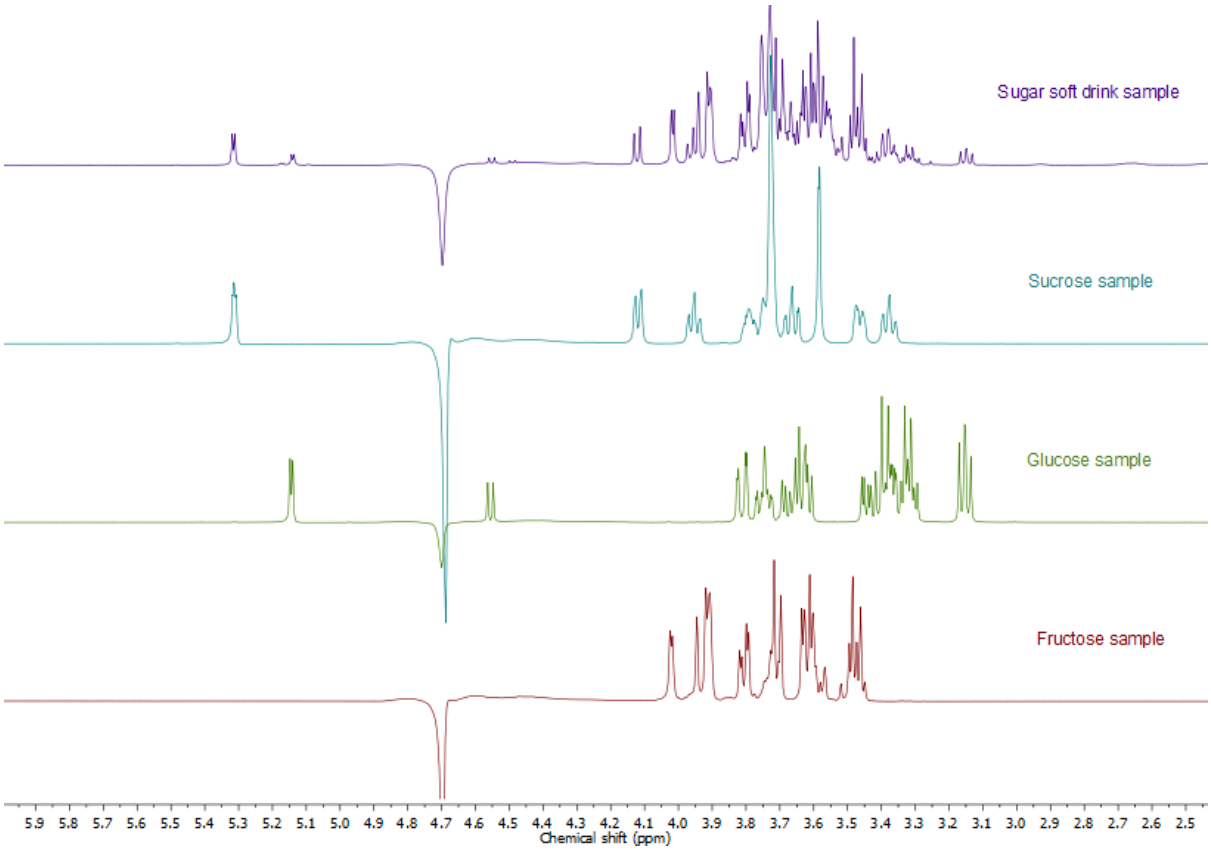

Figure S5. ^{1}H NMR spectra with solvent suppression of a sugar containing soft drink sample (innocent coconut water) with internal standard of different sugar (glucose, fructose, and sucrose, each of them 3.4 g per 100 mL) water solutions. All samples were in water with solvent suppression (water proton close to 4.86 ppm). The peaks at 5.48 ppm and 4.29 ppm (sucrose, 1H), 5.30 ppm and 3.31 ppm (glucose, 1H and 2H respectively) and 4.18 ppm (fructose 1H) are the most distinctive and therefore used here to estimate the ratio of different sugars in the softdrink.